Adding polarimetric imaging to depth map using improved light field camera 2.0 structure

Zhang Xuanzhe*[abc], Yang Yi[ab], Du Shaojun[c] , Cao Yu[c],
[a]Anhui Institute of Optics and Fine Mechanics, Chinese Academy of Sciences, Hefei 230031, China/P. R.China; [b]University of Science and Technology of China, Hefei 230026, China/P. R. China; [c]College of Optoelectric Science and Engineering, National University of Defense Technology, Changsha 410073, China

ABSTRACT

Polarization imaging plays an important role in various fields, especially for skylight navigation and target identification, whose imaging system is always required to be designed with high resolution, broad band, and single-lens structure. This paper describe such a imaging system based on light field 2.0 camera structure, which can calculate the polarization state and depth distance from reference plane for every objet point within a single shot. This structure, including a modified main lens, a multi-quadrants Polaroid, a honeycomb-liked micro lens array, and a high resolution CCD, is equal to an "eyes array", with 3 or more polarization imaging "glasses" in front of each "eye". Therefore, depth can be calculated by matching the relative offset of corresponding patch on neighboring "eyes", while polarization state by its relative intensity difference, and their resolution will be approximately equal to each other. An application on navigation under clear sky shows that this method has a high accuracy and strong robustness.

Keywords: Polarimetric imaging, Depth map, Light field camera 2.0, Computation imaging

1. INTRODUCTION

Polarimetric imaging is an exciting imaging technology which can obtain 2D polarization state distribution of targets in real time. It is particularly suited to 4 applications as follow: 1. Identifying artificial targets from complicated nature environments based on significant difference of polarization property between them two; 2. Identifying targets hidden under camouflage background based on its insensitivity ability to deceptive geometrical patterns; 3. Obtaining clear image through haze or smoke based on high penetrating ability of polarization information; 4. Navigating with skylight under complicated weather based on polarized property of sunlight. The basic principle of such imaging technology is to measure 4 Stokes parameters for each object points, and then calculate polarization state distribution. For nature targets identification, measuring 3 linear polarization parameters is enough because circular polarization of such target is very weak, while for artificial targets identification, all 4 parameters are necessary because circular polarization state is just the most significant difference between targets and background. Through several decades' development, 5 technical solutions have been detailed studied and achieved good results, as shown in Tab 1. However, all 5 technologies cannot work as utility system which should be designed with high resolution, broad band, and robust structure.

This paper describes a structure and algorithm to meet these needs, which is found along with light field studied by our group. It can calculate the polarization state and the depth distance from reference plane for every objet point within a single shot in broad band, and all need to do is just to modify main lens of light field camera with a multi-quadrants Polaroid. The form of multi-quadrants Polaroid is unconstrained, which can be designed with 3 quadrants for linear polarimetric imaging or 4 quadrants for complete polarimetric imaging. Even better, such modification does not much affect the normal use of light field camera, that's to say, depth map can still be extracted from the same data. Obtaining both polarization image and depth map will not only help to get more information of target but also to improve the accuracy for each other, because there is always some object points invalid for one algorithm but valid for the other, and one valid calculation is enough to the other one with correlation estimation. What's more, this polarization imaging methods will be continuous improved along with the light field camera development, because its algorithm has been combined to depth map estimation.

Digital Optical Technologies 2017, edited by Bernard C. Kress, Wolfgang Osten, H. Paul Urbach, Proc. of SPIE Vol. 10335, 103351Q · © 2017 SPIE
CCC code: 0277-786X/17/$18 · doi: 10.1117/12.2270144

Table 1. Development history of polarization imaging

Times	Types	Description	Disadvantage
1970	Rotating polarizer	Work in time series with rotating polarizer in front of a camera	static imaging; average-size
1980	Separation amplitude polarization imaging device	Work asynchronously with Multi cameras behind different polarizer in the same optical path.	Multi cameras; big size; complex structure
1990	Liquid crystal tunable filter polarization imaging device	Work in time series with electric liquid crystal tunable polarizer in front of camera.	Low transmittance; narrow band; electric noise
2000	Separated focal plane polarization imaging device	Calculate complete polarization state using every 4 pixels, with different polarizer in front of each pixel	High assembly difficulty; few pixels for manufacture difficulty
2003	Channel modulated polarization imaging device	Modulate Fourier plane with 4 Stokes parameters	Narrow band; Low transmittance

2. POLARIZED MODULATION WITH LIGHT FIELD CAMERA

2.1 Structure

The polarization imaging camera setup that will be discussed is shown in Fig 1. The main lens generates an image to the right of it. Note that the image may also be virtual in the sense that it is formed behind CCD. The image of the main lens is then projected by the micro lenses onto CCD. A multi-quadrants polaroid is located at pupil, dividing pupil into several separate areas, therefore, a certain imaging channels through one of these polarization area and independent micro lens is established, and pixel in such channel represent a Stokes parameter for corresponding object point.

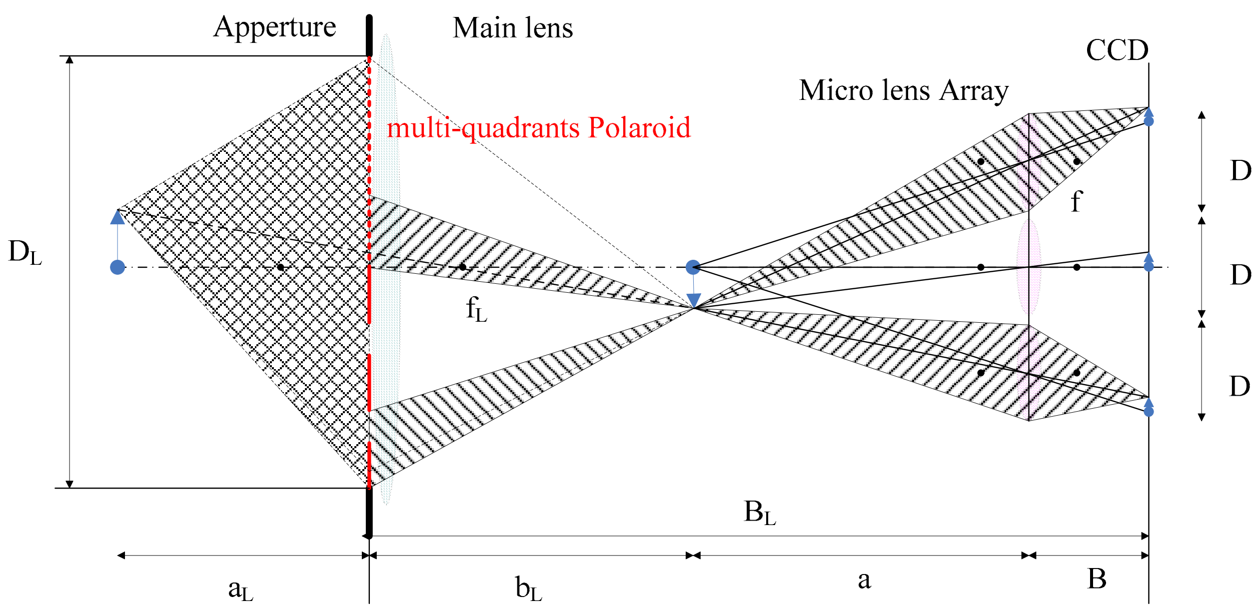

Figure 1. Basic imaging process of polarized modulation camera (1D), Note that Polaroid at pupil has 2 quadrants with 2 different polarization states

The micro images generated by the micro lenses in this system should just touch to make the best use of the image sensor. With respect to Fig 1 this means that

$$\frac{B}{D}=\frac{B_L-B}{D_L}\Leftrightarrow N=N_L-\frac{B}{D_L} \tag{1}$$

Where N is the f-number of the micro lenses and N_L is the f-number of the main lens. Since typically B << D_L, it follows that $N \approx N_L$. That is, the f-numbers of the main imaging system and the micro lens imaging system should match. In this way, the image area of each micro lens will be in same size, and also be divided to 3 or 4 quadrants. Another important concept is that of the virtual depth. Fig 1 can also be regarded as the projection of a real main lens image point onto the camera's image plane by a micro lens centered on the main lens's optical axis. The virtual depth of a main lens image point is defined as follow.

$$v := a / B \tag{2}$$

The number of quadrants depends on application conditions and will decide the algorithm valid rate at the same time. At first, compete polarization state calculation needs 4, which is necessary for artificial target identification from nature background, and linear polarization state calculation only needs 3, if there is no nature object in application. In the second place, less quadrants will lead to higher algorithm valid rate, because the image of quadrants boundary will be blurry, more quadrants means more pixels wasted.

2.2 Standard form

The two limits of the general light field camera are at $f \to \infty$ and f = B. The case $f \to \infty$ is the ordinary camera with an additional flat sheet of glass instead of a micro lens array. The other limit f = B is, what is usually described as the standard light field camera in the literature. The case $f \neq B$ is called light field camera 2.0 or focused light field camera. For standard light field camera, as the micro lenses are focused to infinity, each pixel in a micro image relates to a particular angle of an incoming parallel light bundle. The whole micro image array therefore stands for all of the incoming light direction at different positions. That is to say, each pixel in a micro image come from separated areas of pupil, while image of quadrants boundary will be clear, and every object point polarization state will be successfully calculated. However, its effective resolution ratio is very poor, equal to the number of micro images, shown as follow.

$$R_e=\frac{p}{D}\frac{D_I}{p}=\frac{D_I}{D}, 1\le |v| \le D/s_0 \tag{3}$$

Where D_I denotes the size of the image sensor, and p denotes the side length of a pixel. It is actually only the minimal results of this technology, in most cases, it is not advantageous to choose the distance between the micro lens array plane and the image plane to be exactly equal to the micro lenses' focal length. The micro images will appear blurred over a large range in this setting, which gives bad results for both depth estimation and polarization calculation. Instead, the distance B should differ slightly from f. This gives a larger depth range in which the micro images appear focused.

2.3 Light field 2.0 form

In fact, the difference between standard form and light field 2.0 form is how many "eyes" looked at the same object point. For the former this number is equal to pixel number under each micro lens, which is constant, while for the latter it depends on how many micro lenses have been covered by imaging projection cone for each object point, which is various for different depth. If the total recorded information divided into two parts, one for image resolution and one for depth resolution, the proportion of the two can be adjusted as required in light field 2.0 form. That is advantage, because tens "eyes" is enough for depth estimation and dozens of "eyes" only needed for wave front calculation.

As the optimal effective resolution of a light field camera is proportional to 1/|a|, main image points close to the reference plane will have the highest effective resolution. For the image space in front of the image plane, objects that are closer are resolved with a higher effective resolution than objects that are far away. For the image space behind the image plane that means that objects far away from the light field camera will be resolved with a higher effective resolution than objects close by. This is advantageous, because objects that are close also appear larger, which compensates the loss in effective resolution. With a particular choice of the main lens focal length, the effective resolution on the object can even be kept constant. Therefore, only the case $a \ll -B$ is considered in the following.

A typical light field 2.0 effective resolution is shown as fig 2. It can be seen that ERR (effective resolution ratio) of 2.0 form is higher only in a small area than that of standard form, but that is enough for most application scenarios. The same affects also works on polarization state calculation, except some object points we cannot find enough Stokes parameters for it, because the image of quadrants boundary is extended in this form, and intensities in such area stand for combination of two or more polarized modulation.

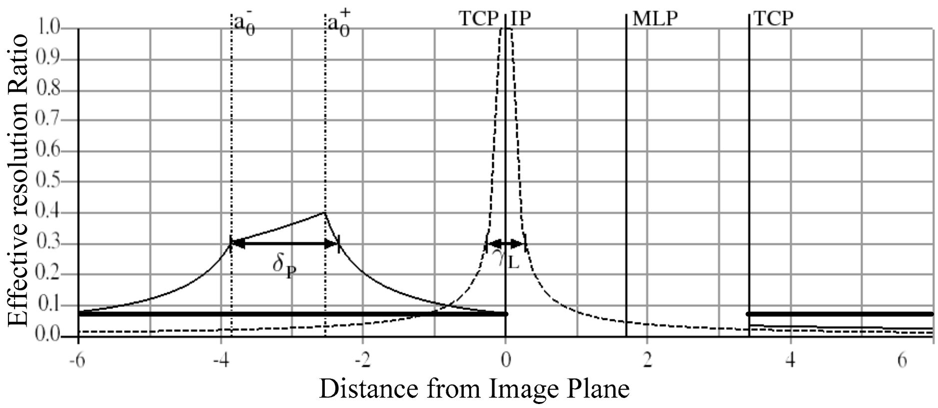

Figure 2. ERR and DOF of main lens and light field 2.0 camera. IP, MLP and TCP indicate positions of image plane, micro lens plane and total covering plane, respectively. Dotted graph is image side ERR of main lens and γ_L is image side DOF of main lens. Solid line graph is ERR of light field 2.0 camera and δ_P is DOF of it, while bold solid line graph is ERR of standard form.

3. INFORMATION EXTRACTION PROCESSING

3.1 Depth map estimation

From a single RAW image of a light field camera the depth of the recorded scene can be estimated, at least at positions with sufficient local contrast. The process can be best understood by regarding the micro lens array as "eyes" array that looks at the virtual image generated by the main lens. As the main lens typically shrinks the object space, the micro lenses "look" at a much smaller version of the original scene. The distance between neighboring micro lenses with respect to this shrunken object space is large enough to offer sufficient parallax for calculating the depth via triangulation. As the distance and orientation of the micro lenses is fixed and assumed to be known, a depth estimation in terms of the virtual depth can be performed without the need of a 3D calibration of the system.

Before a triangulation can be calculated, it has to be known which pixel in neighboring micro images are images of the same object point. This can be done by calculating, for example, the correlation or sum of absolute differences (SAD) of small pixel patches along the epipolar lines of micro image pairs, just as in standard stereo camera approaches. Triangulation is therefore only possible in places with local image contrast, i.e. at edges, corners or other structures.

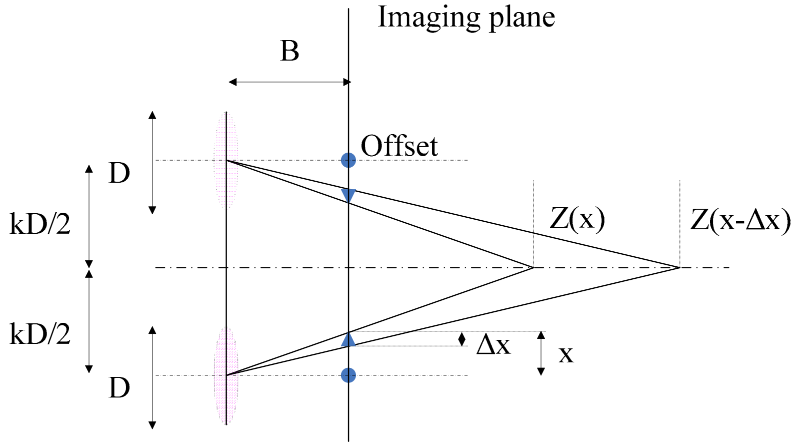

Figure 3. Relation between pixel resolution in micro images and depth resolution (1D)

Figure 3 shows the geometric construction used. An image point at distance x from the micro image center, so called offset, intersects the central bisecting line at point z(x). If Δx is the size of a pixel, then the distance between z(x) and z(x $-\Delta x$) is regarded as the depth resolution for a pixel at distance x from the micro image center. The relation between z and x is given by

$$\frac{z}{\kappa D/2} = \frac{B}{x} \Leftrightarrow z = \frac{1}{x} B \frac{D}{2} \tag{4}$$

The point at distance z(x) from the micro image plane can now be projected back through the main lens into the corresponding object space position a(x) using the thin lens equation. Let z_0 denote the distance of the virtual image plane. Denote the distance between the main lens plane and the total covering plane at z_0 by b_0. The depth positions in object space are then given by

$$a(x) = \left[\frac{1}{f_L} - \frac{1}{b_0 + z(x) - z_0} \right]^{-1} \tag{5}$$

The depth resolution in object space is given as $|a(x) - a(x - \Delta x)|$. From Fig 3 it becomes clear that just as for the lateral resolution, the image side depth resolution of the micro images is higher for far away objects than for close objects. For a given main lens focal length f_L there exists a total focus distance T_L such that the depth resolution is constant over the whole depth range. Let $b_0 = f_L + z_0$, and $a_0 = 1/(1/f_L - 1/b_0)$, then it may be shown by

$$a(x) = x \frac{2 f_L^2}{\kappa D B} + f_L \tag{6}$$

One special property of a light field camera is that a point is seen in more and more micro images as |v| increases. Therefore, the depth of a scene does not have to be evaluated by only utilizing directly neighboring micro images. Instead, the micro images with the largest separation that still have an image of the same point, can be used. Usually, we used the pair on outmost circle, the parameter κ introduced in Fig 3 is a measure of the distance between the pair centers. In fact, z is minimal in Fig 3 if x = D/2. In that case, κ = z/B = v, where v is the virtual depth. In other words, κ gives the minimal virtual depth for which a triangulation can be performed. For a hexagonal micro lens array the first ten consecutive κ values for micro lens pairs are: 2.0, 3.5, 4.0, 5.3, 6.0, 6.9, 7.2, 8.0, 8.7, 9.2, 10. For scenes with a lot of fine structure and good contrast, the disparity of corresponding pixels patches can be calculated with up to a tenth of a pixel accuracy.

3.2 Polarization imaging calculation

As described above, depth map is calculated by offset x and factorκof a series of pixels imaging from the same object point, and intensities of these pixels are supposed equal to each other. After multi quadrants polarizer has been located on pupil, these intensities have a chance to be modulated by different polarizer, because a little blurry pupil image will be superimposed to every micro image, and divide micro image into multi quadrants too. If image pixels of the same object point can be find at least one in every quadrant, polarization state will be successfully calculated. As shown in Fig 3, x is offset from the micro image center, z(x) is depth from reference plane, and I(x) is the intensity of such pixel, which can be used for calculating the polarization pattern (AOP and DOP) with Stokes' equations. The Stokes vector S contains 4 components, also needing 4 measurable physical values to be calculated. For nature target identification, measuring 3 linear polarization parameters is enough because circular polarization of such target is very weak, while for artificial target identification, all 4 parameters are necessary because circular polarization state is the most significant difference between target and background. Figure 4 shows the multi quadrants polarizer may used.

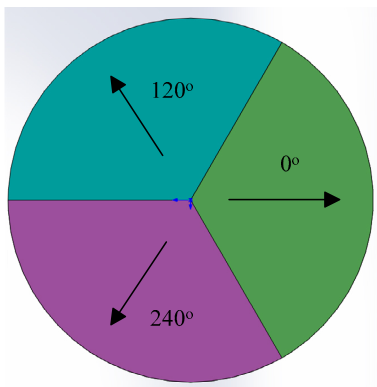

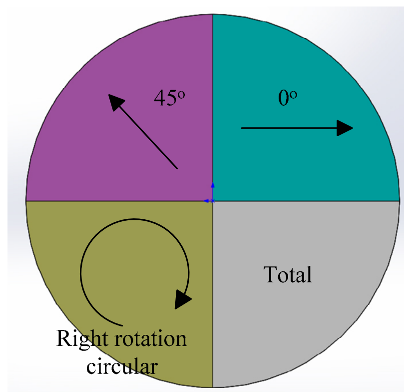

Figure 4. 3quadrants polarizer for linear polarization state calculation and 4quadrant polarizer for complete polarization state calculation

Complete polarization calculation

Once all 4 intensities respectively come from 4 quadrants be obtained, shown on the right of Fig 5, the polarization pattern can be computed with the equations (7) easily. Note DOP stands for Degree of Polarization.

$$\begin{cases} S_0 = I_{TOTAL} = I \\ S_1 = I_{0^o} - I_{TOTAL} = IP\cos 2\psi \cos 2\chi \\ S_2 = I_{45^o} - I_{TOTAL} = IP\sin 2\psi \cos 2\chi \\ S_3 = I_{rotation} - I_{TOTAL} = IP\sin 2\chi \end{cases}$$
$$DOP = \frac{\sqrt{{S_1}^2 + {S_2}^2 + {S_3}^2}}{S_0} \tag{7}$$

Linear polarization calculation

To get higher accuracy and more fault tolerance, a symmetric structure has been adopt in 3 quadrants polarizer, as shown on the left of Fig 5. Angles of polarization in 3 quadrants are 0°, 60°, and 120°, and the output intensities are marked as $I_{0°}$, $I_{60°}$, $I_{120°}$, respectively. The relation between S and I is given by Eqs (8), and the polarization state can be calculated by equation (9), where AOP stands for Angle of Polarization.

$$\begin{cases} S_0 = I = \dfrac{2}{3}\left(I_{0^o} + I_{120^o} + I_{240^o}\right) \\ S_1 = \dfrac{2}{3}\left(2I_{0^o} - I_{120^o} - I_{240^o}\right) \\ S_2 = \dfrac{2}{\sqrt{3}}\left(-I_{120^o} + I_{240^o}\right) \end{cases} \tag{8}$$

$$DOP = \frac{\sqrt{S_1{}^2 + S_2{}^2}}{I};\ AOP = \frac{1}{2}\arctan\left(\frac{S_1}{S_2}\right) \tag{9}$$

As the structure is modified from light field camera 2.0, polarization calculation process is very similar with depth map estimation, and the resolution is expected to approach to that of light field 2.0, almost 10% of the CCD resolution.

3.3 Algorithm summary

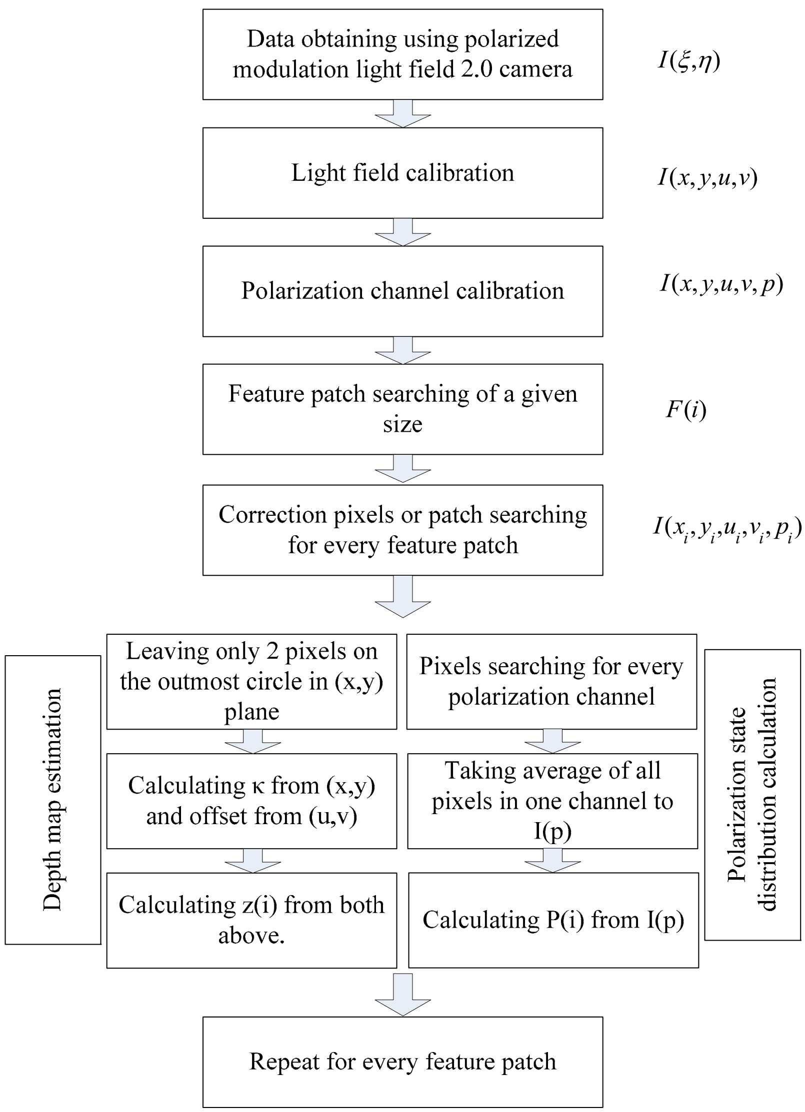

Figure 5. Calculation process schematic diagram

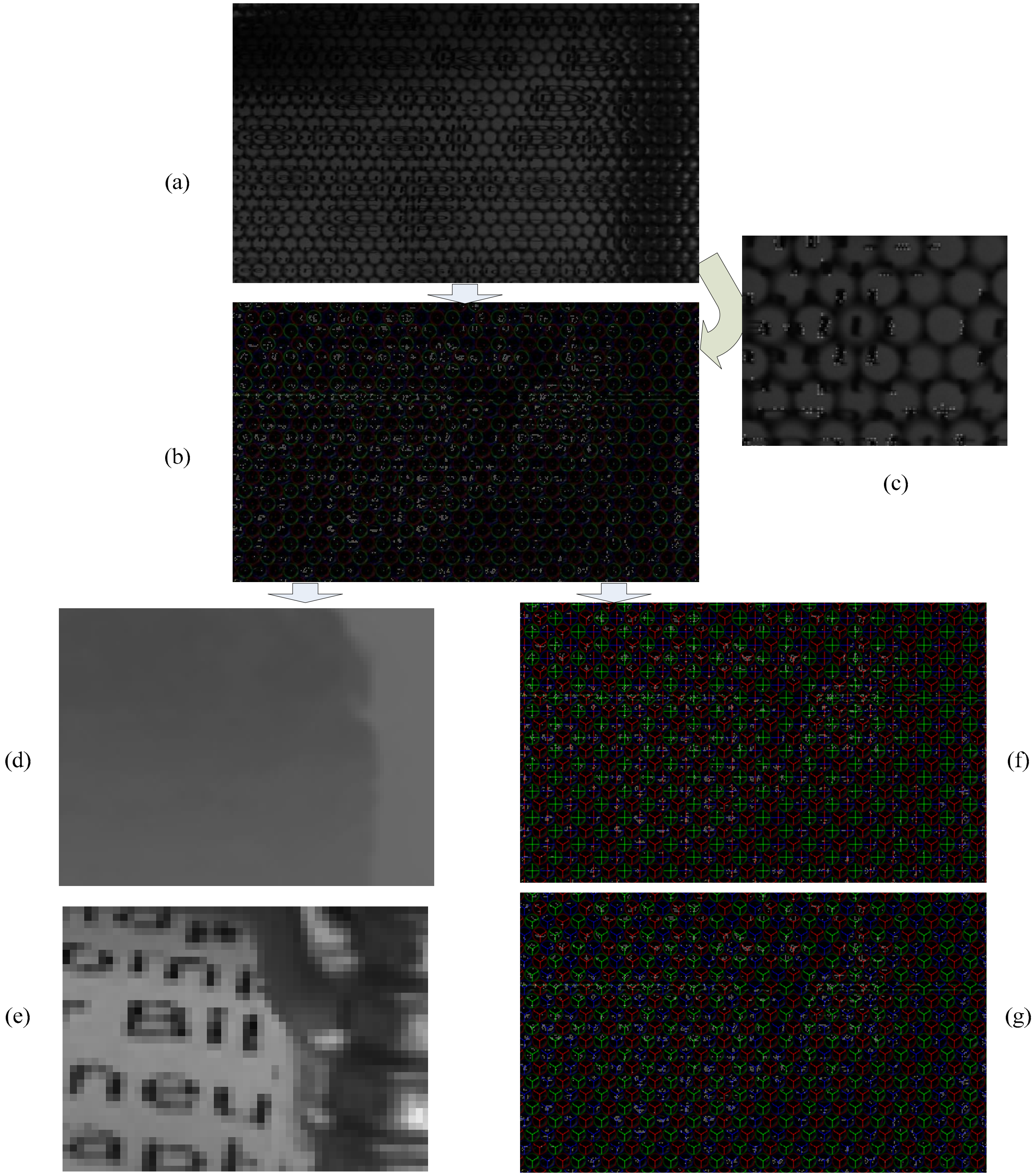

Figure 6. Calculation process with image example: (a) RAW image data; (b) light field calibration and feature patch searching; (c) feature patch searching example; (d)depth map estimation; (e) 4 channels calibration for complete polarization state calculation; (f) 3 channels calibration for linear polarization state calculation

4. APPLICATIONS OF NAVIGATION

Experiments were carried out using modified Raytrix light field camera, which has 3 types of focal lengths in micro lens array, so called light field 2.5. Such camera has longer depth of field than that of 2.0, but the information extraction processing is completely the same. The resolution of the light field camera (type: Raytrix-R29) is 6576 × 4384. The micro lens array has 205 × 137 micro lenses, and each of them covers 32 × 32 pixels beneath. Fig 7 shows the experimental platform. A series of experiments were carried out under different daytime weather conditions such as clear, cloudy, foggy, and hazy to test the precision and performance of our method and system. This paper only presents clear sky experiment results.

Figure 7. Experiment platform and clear sky

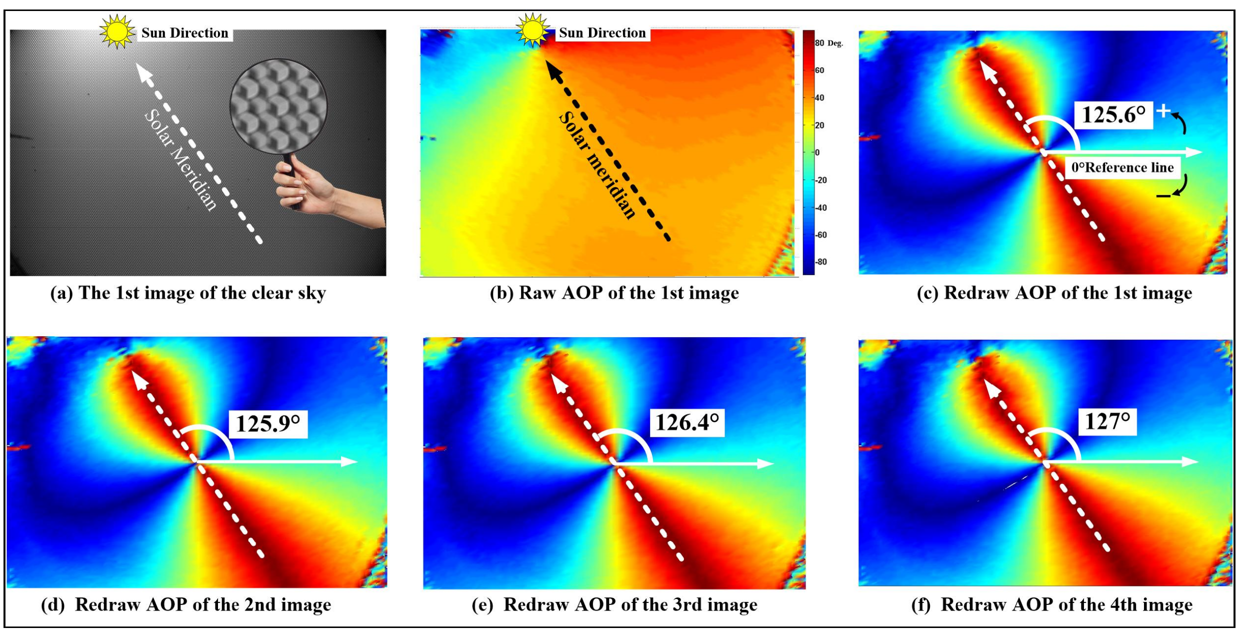

Figure 8. Linear polarization imaging in clear sky: (a) RAW image data and sub-images behind the micro lens for linear polarization calculation, which has been divided into three parts with different pixel gray; (b) raw image of AOP data; (c) redrawn image of (b). The symmetric feature of the polarization pattern with respect to the sun meridian is shown clearly. We defined the horizontal rightward direction as the reference direction of 0° and counterclockwise rotation as positive for

the course angle calculation. (d)~(f) are three other images of experimental results with the same time interval, and the calculated values of course angle are labeled.

Figure 8 gives the photograph of the sky, the image of AOP, and the calculated value of the course angle. The camera took four images of the sky every 4 min without movement, and the results are calculated with every four frames of image to improve accuracy. Since the time interval is only about 4 min, and the azimuth angle of the sun changes 15° each hour, therefore the theoretical variation of the sun direction between every two consecutive images is about 0.5° according to our time and location, which is too small to be distinguished by human eyes. However, in our results, each calculated image is really rotated slightly in the same direction and the angle variation between every two adjacent images is just 0.5°. It shows that this method is particularly appropriate for navigation with high accuracy, broad band and strong robustness.

5. CONCLUSION

As has been discussed above, both polarization image and depth map can be extracted in one shot using polarized modulated light field camera. The resolution of former will approach to that of latter, which is about 5%~ 10% of 2D CCD pixels amount in light field 2.0+ form (eg. Raytrix). The structure is very robust, because there is no wavelength limitation, no moving parts, and all need to do is to modify main lens of light field camera with a multi-quadrants Polaroid. All of these advantages are owe to the nice nested structure, which is also help to deeply understand light field camera. Further research of this nested structure application is being carried out by our group.

REFERENCES

[1] Perwass, Christian, and Lennart Wietzke. "Single lens 3D-camera with extended depth-of-field." *IS&T/SPIE Electronic Imaging*. International Society for Optics and Photonics, (2012).

[2] Zhang, Wenjing, et al. "Angle of sky light polarization derived from digital images of the sky under various conditions." *Applied Optics* ,56.3: 587-595 (2017)

[3] Suhai, Bence, and Gábor Horváth. "How well does the Rayleigh model describe the E-vector distribution of skylight in clear and cloudy conditions? A full-sky polarimetric study." *JOSA A* ,21.9: 1669-1676 (2004)

[4] Tao, Michael W., et al. "Depth from combining defocus and correspondence using light-field cameras." *Proceedings of the IEEE International Conference on Computer Vision*,(2013).

[5] Konnen, G. P.[*Polarized light in nature*] CUP Archive, (1985).

[6] Zhang, Xuanzhe, Bohong Shu, and Shaojun Du. "3D imaging of translucent media with a plenoptic sensor based on phase space optics." *SPIE Optics+ Optoelectronics* International Society for Optics and Photonics, (2015).

[7] LISHJ, JIANGHL. "Developmentstatusandkeytechnologiesofpolarizationimagingdetection." *Chinese Optics,* 6.6: 803 (2013)

[8] Apelt, Federico, et al. "Phytotyping4D: a light - field imaging system for non - invasive and accurate monitoring of spatio - temporal plant growth." *The Plant Journal* , 82.4: 693-706 (2015)

[9] Bechis, K., and A. Pitruzzello. "Research into a Single-Aperture Light Field Camera System to Obtain Passive Ground-based 3D Imagery of LEO Objects." *Advanced Maui Optical and Space Surveillance Technologies Conference*, (2014)

[10] Perez, Carlos Cruz, et al. "Calcium neuroimaging in behaving zebrafish larvae using a turn-key light field camera." *Journal of Biomedical Optics,* 20.9: 096009-096009 (2015)

[11] Goulet, Mathieu, et al. "Novel, full 3D scintillation dosimetry using a static plenoptic camera." *Medical physics,* 41.8 (2014).

[12] Shademan, Azad, et al. "Supervised autonomous robotic soft tissue surgery."*Science translational medicine,* 8.337: 337ra64-337ra64 (2016)

[13] Zeller, N., F. Quint, and U. Stilla. "Calibration and accuracy analysis of a focused plenoptic camera." *ISPRS Annals of the Photogrammetry, Remote Sensing and Spatial Information Sciences,* 2.3: 205 (2014)